Accepted Manuscript

Scaling Effects in the Mechanical Response of Sandwich Structures Based on Corrugated Composite Cores

J. Zhou, Z. Guan, W.J. Cantwell

PII: S1359-8368(16)30015-4

DOI: 10.1016/j.compositesb.2016.02.061

Reference: JCOMB 4099

To appear in: *Composites Part B*

Received Date: 18 January 2016

Revised Date: 15 February 2016

Accepted Date: 24 February 2016

Please cite this article as: Zhou J, Guan Z, Cantwell WJ, Scaling Effects in the Mechanical Response of Sandwich Structures Based on Corrugated Composite Cores, *Composites Part B* (2016), doi: 10.1016/j.compositesb.2016.02.061.

Scaling Effects in the Mechanical Response of Sandwich Structures Based on Corrugated Composite Cores

J. Zhou[1], Z. Guan[1] and W.J. Cantwell[2]

[1] School of Engineering, University of Liverpool, Liverpool, L69 3GH, U.K.

[2] Department of Aerospace Engineering, Khalifa University of Science, Technology and Research (KUSTAR), Po.Box127788, Abu Dhabi, UAE.

Abstract

This paper investigates the compression response of all-composite sandwich structures based on glass fibre/epoxy and carbon fibre/epoxy cores. The structures were manufactured by wrapping layers of composite prepreg around a series of adjacent steel cylinders. Prepreg surface layers were then attached to the upper and lower surfaces of these wrapped cylinders and the entire structure cured in a hot press. Co-curing the skins and the corrugated core in this fashion ensured a strong bond in the critical skin-core interfacial region. The mechanical response of the sandwich structures was modeled using the finite element method.

Initial attention focuses on investigating the effect of varying key geometrical parameters, such as the corrugation thickness and the number of unit cells, on the mechanical properties of the sandwich structures. The failure mechanisms during compression loading are discussed and compared with the numerical predictions from the finite element models.

The second part of this study investigates scaling effects in the compression response of both the carbon and glass fibre-based sandwich structures. In this part of the study, the geometry of the sandwich structures, as well as the relevant testing conditions, were varied in order to ensure a consistent scaling approach. Here, variations in compression strength as well as changes in failure mode were investigated with increasing scale size.

Keywords:

Sandwich structure, compression, scaling, corrugated core

Introduction

Lightweight sandwich structures are finding increasing use in a wide range of lightweight aerospace designs. Typically, such structures are based on composite skins bonded to a low density core material, such as a honeycomb or a closed cell foam [1-3]. More recently, there has been a growing interest in the development of high-performance sandwich panels containing novel core designs, such as those based on advanced periodic designs, including truss, lattice and prismatic structures [4-8]. For example, Xiong *et al* [7] used electrical discharge machining to manufacture three dimensional lattice cores based on a carbon fibre reinforced epoxy. The sandwich panels were subjected to flatwise compression and the resulting data compared to analytical predictions [7]. Yin *et al* [8] developed what are termed stretch-stretch hybrid hierarchical composite cores based on composite pyramidal lattice sandwich panels in macroscopic truss designs. Zuhri *et al* [9] employed the slotting technique proposed by Coté *et al* [10] to manufacture square and triangular honeycomb cores based on natural fiber composites. They showed that the square honeycomb structure exhibited compressive properties that greatly exceed those based on triangular designs.

In recent years, there has been an increasing interest in the possibility of employing corrugated composite panels in the design and manufacture of morphing structures and energy-absorbing components [11-14]. Kazemahvazi *et al* [14] investigated the compression and shear properties of hierarchical corrugations based on a carbon fibre reinforced epoxy resin. The resulting panels exhibited different failure modes as the geometry of the structure was varied. More recently, corrugated core materials based on both glass and carbon fiber reinforced epoxy composites have been developed and tested [15]. Here, the compression molding technique, employing a steel mould with a triangular profile, was used to produce a range of systems with differing wall thicknesses. The mechanical response of the composite sandwich structures were compared to that offered by an all-aluminium system, where it was shown that the specific compression strength of a carbon fiber-based core exceeded that of its metallic counterpart [15]. Malcom *et al* [13] manufactured and tested a range of novel foam-filled and plain corrugated core structures based on 3D glass fiber fabrics. The compressive response of the panels was investigated as a function of the strut aspect ratio and compared to the predictions of a micromechanical model. It was shown that slender struts failed by elastic buckling, whereas thicker struts failed due to plastic

microbuckling [13]. Jin *et al* [16] conducted compression, shear and flexural tests on what are termed integrated woven corrugated sandwich composites. The authors showed that the compressive properties of these sandwich structures, based on wave-like composite cores, exhibit strength and stiffness properties that scale with the square of the relative density.

Schneider *et al* [17] investigated the quasi-static and dynamic compression properties of sandwich panels based on self-reinforced PET corrugated cores. The authors showed that whereas the parent material displayed a small degree of rate-sensitivity, the cores exhibited a much greater level of rate-sensitivity. This was attributed to micro-inertial stabilisation of the core struts, as well as an increased plastic tangent stiffness of the self-reinforced composite.

The aim of the present study is to manufacture and evaluate the mechanical properties of all-composite sandwich structures based on corrugated composite cores. Here, a simple tube-wrapping technique is used to produce cores based on a repeating sinusoidal design. Attention focuses on establishing the effect of varying key geometrical parameters on the compression response of the sandwich structures. Observed trends in the experimental data are compared to numerical predictions resulting from a series of finite element models.

Experimental procedure

The sinusoidal-shaped composite cores investigated in this study were manufactured using a woven glass fibre reinforced plastic (GFRP), and a woven carbon fibre reinforced plastic (CFRP). The nominal thicknesses of the GFRP and CFRP prepregs were 0.125 and 0.25 mm respectively. Details of the cure cycles and mechanical properties of these two materials are given in Tables 1 and 2. The core structures were manufactured by wrapping sheets of composite prepreg around an array of Teflon-coated steel tubes, as shown schematically in Figure 1(a). In the initial part of this investigation, tubes with a diameter of 20 mm were used. Five thicknesses of corrugation, shown as 't' in Figure 1(b), were obtained by wrapping between one and five plies of CFRP, and between two and ten plies of GFRP, around the tubes. The facesheets of the sandwich panels were introduced by laying composite plies on the upper and lower surfaces of the uncured tubular array. Table 3 gives the key dimensions of the sandwich structures investigated in this part of the study.

Following the laying-up procedure, the entire structure was cured in a hot press according to the processing parameters given in Table 1. Here, the panels were heated to 125 ^{o}C at a heating rate of 1.5 ^{o}C/minute. This temperature was then maintained for 90 minutes, before switching off the press and allowing the samples to cool to room temperature. The sandwich panels were then removed from the press and post-cured for 90 minutes at 125 ^{o}C.

Test specimens were prepared by removing samples from the manufactured panels. Here, the majority of tests were undertaken on samples containing two cells, as shown in Figure 2(a). An examination of the figure highlights the presence of a depression along the lower surfaces of the samples, where the cylinder impinged on the composite. Subsequent testing showed that failure always occurred at locations well away from these points, suggesting that their effect was minimal. The nominal length and width dimensions of the two-cell samples were 80 and 20 mm respectively, and the heights of the samples varied between 20.75 and 23.75 mm, depending on the thickness of the corrugation, t.

In order to ensure that the mechanical response of the two cell geometries was representative of a larger structure, an additional series of tests was undertaken to study the influence of varying the number of unit cells in the test samples. Test specimens based on between one and five unit cells and a cell diameter of 20 mm were manufactured. The nominal thicknesses of the composite in the skin and core materials was 0.5 mm.

Compression tests on the sandwich panels were carried out using an Instron 4045 universal test machine. The tests were undertaken at a crosshead displacement rate of 1 mm/min. The samples were photographed during testing in order to elucidate the modes of failure and fracture.

Scaling effects in the mechanical properties of the cores were investigated in the final part of this study. Here, steel tubes with diameters of 40n mm were used, where n is the scale size, taken as ¼, ½, ¾ and 1 in this study. The thickness of the core corrugation was also varied in order to ensure that scaling laws were respected. Here, 8n layers were used to produce the GFRP samples (i.e. 2 plies for the smallest scale size, four for the n=1/2 structure, etc.). Scaling of the CFRP samples was ensured by wrapping 4n plies for each of the four scale sizes. As before, each sample was based on two unit cells, as shown in Figure 2(a). The thickness of the skins in each panel was also scaled in order to ensure that it was equal to that of the thickness of the corrugation in that sample. The length and width of the test samples were 160n mm and 40n mm respectively. Details of the geometries of the four scales sizes are given in Table 3 and Figure 2(b) shows photographs of the four scale sizes of CFRP sandwich panel.

Compression tests on the scaled sandwich structures were conducted on the previously-discussed Instron 4045 test machine. In this case at a crosshead displacement rate of 4n mm/min were employed during testing. Potential changes in failure mode with increasing scale size were recorded by taking photographs at regular intervals during the test.

Numerical Procedure

Numerical models were developed to simulate the compression response of the corrugated core sandwich structures subjected to quasi-static loading. The composite was modeled using user-defined Hashin's 3D failure criteria for an anisotropic composite material. Figure 1(c) shows the finite element mesh of a test specimen. Here, the curvilinear core and skins were meshed using eight-noded solid elements with reduced integration (C3D8R). The size of the FE models was selected to correspond to test specimens. Mesh sensitivity was studied by varying the mesh density within the plane and through the thickness of the composite sheet. Based on the results of this study, a mesh size of 1 x 1 mm within the plane and two elements through the thickness of

composite core were used. A number of interfaces were considered in the model, including that between the face sheet and the loading platen, those between the composite contoured core and the face sheets, as well as the possible self-contact between members of the contoured core. The material properties of the GFRP and CFRP composites are given in the Table 2. The modified 3D failure criteria [18, 19] were used to simulate the overall response of the sandwich structures in a Cartesian coordinate system (x, *y*, z). The failure criteria, together with the related constitutive model, were then implemented into the ABAQUS/Explicit using a subroutine [20, 21], which can be expressed as follows:

Fibre tension: $(\sigma_{11}>0)\ F_f^t=\left(\frac{\sigma_{11}}{X_{1t}}\right)^2+\left(\frac{\sigma_{12}}{S_{12}}\right)^2+\left(\frac{\sigma_{13}}{S_{13}}\right)^2,\ d_{ft}=1$ (Eq. 1)

Fibre compression: $(\sigma_{11}<0)\ \frac{|\sigma_{11}|}{X_{1t}}, d_{fc}=1,\ d_{fc}=1$ (Eq. 2)

Matrix tension: $(\sigma_{22}+\sigma_{33}>0)\ \frac{(\sigma_{22}+\sigma_{33})^2}{X_{2t}^2}+\frac{\sigma_{23}^2-\sigma_{22}\sigma_{33}}{X_{23}^2}+\frac{\sigma_{12}^2+\sigma_{13}^2}{X_{12}^2}=1,\ d_{mt}=1$ (Eq. 3)

Matrix compression: $(\sigma_{22}+\sigma_{33}<0)\left[\left(\frac{X_{2c}}{2S_{23}}\right)^2-1\right]\frac{(\sigma_{22}+\sigma_{33})}{X_{2c}^2}+\frac{(\sigma_{22}+\sigma_{33})^2}{4S_{23}^2}+\frac{\sigma_{23}^2-\sigma_{22}\sigma_{33}}{X_{23}^2}+\frac{\sigma_{12}^2+\sigma_{13}^2}{X_{12}^2}=1,\ d_{mc}=1$ (Eq. 4)

where X_{1t}, X_{1c}, X_{2t}, X_{2c}, S_{12}, S_{13} and S_{23} are the strength components and d_{ft}, d_{fc}, d_{mt} and d_{mc} are the damage variables associated with the four different failure modes. Given that Abaqus/Explicit was employed, different time durations were studied to identify that with a minimized rate-dependence, this being 0.1 s. The behaviour of the material system following damage initiation was defined using:

$$\sigma_{ij}=C_{ij}(d)\cdot\varepsilon_{ij} \quad \text{(Eq. 5)}$$

where $C_{ij}(d)$ is the degradation matrix.

Results and Discussion

The Influence of Cell Number

Figure 3 shows typical stress-strain curves for glass fibre/epoxy corrugations based on increasing numbers of unit cells. An examination of the figure indicates that all of the curves are very similar and appear to collapse onto what is effectively a unique trace. In all cases, the stress initially increases in a linear fashion, before reaching a maximum and dropping sharply to a steady-state value. In the final stages of the test, the stress begins to increase once more as the corrugation begins to densify.

Figure 4 summarises the influence of the sample width (i.e. the number of unit cells) on the compression strength of both the glass and carbon fibre corrugations. It is interesting to note that there is little difference between the smallest and largest samples, with the strength of a single unit cell being effectively the same as that of a more representative section of the sandwich structure. These results are encouraging and suggest that the two unit cell geometries used in the remainder of this paper adequately reflect the overall properties of these sandwich structures. For this particular combination of web thickness and cell diameter, it is clear that the carbon fibre composites out-perform their glass-based counterparts, with the former offering compression strengths that are roughly double those of the glass fiber reinforced epoxy panels.

The Influence of Corrugation Thickness

Figure 5(a) shows typical stress-strain traces following compression tests on GFRP samples with corrugation thicknesses ‘t’ between 0.25 and 1.25 mm. As expected, increasing the value of ‘t’ serves to increase the compression strength of the core. The strength of the thinnest core is clearly very low, reaching a value 0.1 MPa before dropping to a value close to zero. Increasing the value of ‘t’ to 0.5 mm results in a similar load-displacement, with the maximum value reaching 0.3 MPa, before dropping to a lower value, as the core buckled under continued compressive loading. Further increases in thickness precipitated a change in the shape of the stress-strain trace, with the curves exhibiting several peaks before the onset of final densification. This is most pronounced in the thickest sample, where the stress initially increases to 2.0 MPa before reducing and then increasing a second time to 1.6 MPa and finally to a peak at 0.5 MPa prior to the onset of densification. The

presence of these peaks in the stress-strain curve is associated with the corrugation flattening against the upper and lower skins, an effect that will be discussed further below.

Figure 5(b) shows typical stress-strain traces for the CFRP samples. An initial examination of the figure indicates that the CFRP cores, in most cases, are much stronger than their GFRP counterparts. However, as before, those samples based on thin walls fail at very low stresses, exhibiting a single peak prior to failure. Increasing the corrugation thickness to 0.75 mm precipitates a change in failure mode, with the resulting trace exhibiting two distinct peaks prior to the an almost complete loss of load-bearing capability. The 1.0 mm thick sample exhibits two distinct peaks and the thickest specimen exhibits a number of increasing peaks prior to failure at a strain of approximately 0.6.

The failure modes observed in GFRP samples with web thicknesses of 0.25, 0.75 and 1.0 mm are shown in Figure 6. Initial deformation in the 0.25 mm thick samples is associated with the flattening of the webs against the surface skins, followed by buckling of one side of the unit cell. This deformation mechanism leads to creasing and fracture of the corrugation (highlighted by the black arrows), precipitating the drop in load observed in the stress-strain curve. Failure in the 0.75 mm thick samples involved initial buckling and creasing close to the upper skin (see arrows), followed by a buckling failure of the webs at their mid-points (also arrowed). This two stage process, i.e. initial creasing followed by reorientation of the struts that ultimately failed in buckling resulted in the two peaks observed in the loading trace. Finally, failure in the 1 mm thick samples involved the formation of a clear 90 degree hinge at the top surface and the vertical alignment of the webs. These re-aligned webs were capable of supporting significant load before failing, leading to the second distinct peak in the stress-strain trace. Figure 7 compares the failure mechanisms in the CFRP samples with the predictions offered by the FE model. Agreement between the predictions and experimental observations is generally good, with the model predicting buckling in the walls of the core, flattening of the core against the upper and lower skins as well as localized creasing of the composite.

The results of the compression tests on the GFRP and CFRP cores are summarized in Figure 8. For purposes of clarity, the values of the thinnest samples have been offset slightly from their nominal values. From the figure it

is clear that the compression strength increases in a non-linear fashion as 't' increases. For example, increasing the corrugation thickness from 0.25 to 1.25 mm results in a sixty-seven fold increase in the compression strength of the GFRP samples. The corresponding increase is even greater for the CFRP samples. From the figure, it is clear the carbon fibre-based core out-performs its glass fibre counterpart, with the difference in strength increasing as the corrugation thickness 't' is increased. In addition, it is worth noting that the densities of the CFRP cores were lower for a given value of 't', suggesting that the relative performance of the carbon fibre systems is even more impressive than that shown in the figure. These trends in compression strength with corrugation thickness mirror those observed following compression tests on corrugated core materials [15].

Jin *et al* [16] stated that the compression strength of corrugated composite structures varied with the square of the relative density of the core. Similarly, Zhang *et al* [22] investigated the compression response of sinusoidal corrugated structures based on stainless steel and developed an analytical solution to model failure through the formation of plastic hinges. The authors showed that the normal compression strength of the core varies with the yield strength of the base material according to the square of (h_c/H_c) where h_c is the thickness of the corrugation and H_c the height of the core. Figure 9 presents plots of compression strength versus the square of (h_c/H_c) for both types of core. From the figure, it is evident that the compression properties do, for a given material system, appear to loosely follow a relationship based on the square of h_c/H_c. Also included in the figure are the scaling data that will be discussed below. Differences in the slopes of the two traces reflect distinct differences in mechanical properties of the two types of composite.

Scaling Effects in the Compressive Properties of the Cores

The effect of varying the specimen size (whilst keeping all of the relative dimensions constant) on the compressive properties of the GFRP and CFRP cores was assessed by undertaking tests on the GFRP and CFRP similar to the geometries shown in Figure 2(b). The tests were undertaken at a constant scaled crosshead displacement rate of 4n mm/minute. Figure 10(a) shows typical load-displacement traces following compression tests on the four scaled sizes of GFRP core. All four traces exhibit similar trends, with the four curves increasing to a maximum before reaching a peak and subsequently dropping sharply. Continued loading of the four samples results in an intermediate loading regime, wherein failure of the cores occurs at relatively low levels of force.

The final region of each load-displacement trace is associated with a rapid rise in force, due to crushing of core and effective densification of the sample.

The load-displacement traces for the GFRP samples in Figure 10(a) were then normalised whereby the force was divided by the square of the scale size (i.e. n^2) and the displacement by the scale size, n. The resulting normalised traces for these glass-based samples are shown in Figure 10(b). An examination of the figure indicates that the four curves appear to collapse onto a relatively unique trace. The maximum force values as well as the densification thresholds are similar for all four samples. Closer inspection indicates that the second distinct peak in the load trace for the n=1/2 sample is not reproduced in the other samples. This may simply be due to sample-to-sample variations in the local failure mode. The evidence in this figure suggests that the compression properties of these GFRP samples obey a simples scaling law and that such an approach can be employed to predict the response of larger structures.

Figure 11 shows the scaled load-displacement traces following compression tests on the CFRP cores. All of the cores exhibit a similar trend, with the force increasing to a maximum before decreasing steadily to a plateau value. Finally, the force increases rapidly during the crushing and densification phases of the test. The figure indicates that the strength of the smallest sample is slightly lower than that of its larger counterparts. This will be discussed in more detail below. Typical photographs of the four scaled sizes of glass and carbon/epoxy core subjected to a scaled displacement of approximately 3/n mm are shown in Figure 12. A comparison of the four GFRP samples suggests that the failure modes are similar in all four scaled sizes, with cells failing in buckling resulting in a sideways instability. Similar observations are apparent in the CFRP samples, with the webs tilting sideways as the load is applied. It is encouraging to note that the failure modes are similar in all four scale sizes of both types of composite, suggesting that simple scaling procedures can be applied to predict the response of these structures.

Figure 13 summarises the influence of scale size on the compression strength of the curvilinear cores. An examination of the figure highlights an absence of any appreciable size effect in the compressive properties of the glass fibre-based material. Here, the compression strength of the GFRP core is roughly constant over the range of specimen sizes, with the strength averaging approximately 0.45 MPa. In contrast, the compression strength of the carbon based cores increases slightly with scale size. For example the compression strength of the

¼ scale sample is 0.4 MPa whereas the strength is equal to 0.5 MPa, when n = 1. It is believed that the size effects apparent in the CFRP data in Figure 12 are associated with the dimensions of the relatively coarse weave in this material. The unit cell in the carbon-based system is approximately 0.8 by 0.8 mm, whereas for the GFRP material this reduces to 0.2 by 0.2 mm. Given that the n = ¼ CFRP system is only based on one ply and the height of the core is just over ten times the length of the weave, local variations in the weave characteristics are likely to be much greater in the smallest sample than for the case where n = 1, in which there are four plies with a core height that is approximately 55 times that of the weave size. It is likely, therefore, that local irregularities in the weave structure will have a much greater effect in the smaller samples. Given that the GFRP weave is much finer, size effects associated with variations in the fabric dimensions are less likely. The results in Figure 13 suggest that scaling techniques similar to those outlined here can be successfully used to obtain an initial estimation of the response of larger, more-representative structures.

Conclusions

A range of all-composite sandwich structures based on a corrugated core have been manufactured by compression molding an array of wrapped metallic cylinders. Tests on the resulting samples indicated that the compression strength increased rapidly with the thickness of the corrugation. The stress-strain traces for the thicker samples exhibited more than one peak, failure mechanisms that were associated with buckling of the web, the formation of a hinge and the re-orienting of the individual webs. The carbon fiber reinforced corrugated structures offered superior compressive properties to its glass-based counterpart, particularly at higher values of corrugation thickness. The finite element model accurately predicted the compressive properties of the sandwich structures, successfully predicting the observed failure mode in most cases. The final part of this study focused on investigating the scaling response of the glass and carbon/epoxy structures. No significant scaling effects were observed in the four scaled sizes, with all four load-displacement curves collapsing onto a relatively unique trace following the normalization process. This evidence suggests that a simple scaling approach can be used to accurately predict the response of more representative sandwich structures.

References

[1]. L. J. Gibson and M. F. Ashby, Cellular solids: Structure and Properties. 2nd ed. Cambridge University Press, 1997.

[2]. M. Daniel and O. Ishai, Engineering Mechanics of Composite Materials. Oxford University Press, 1994.

[3]. D. T. Queheillalt and H. N. G. Wadley, Pyramidal lattice truss structures with hollow trusses. Materials Science and Engineering A 2005;397:132–137.

[4]. F. W. Zok, H. J. Rathbun, Z. Wei, and A. G. Evans, Design of metallic textile core sandwich panels. International Journal of Solids and Structures 2003; 40:5707–5722.

[5]. S. Chiras, D. R. Mumm, A. G. Evans, N. Wicks, J. W. Hutchinson, K. Dharmasena, H. N. G. Wadley and S. Fichter, The structural performance of near-optimized truss core panels. International Journal of Solids and Structures 2002;39: 4093–4115.

[6]. J. Wang, A. G. Evans, K. Dharmasena and H. N. G. Wadley, On the performance of truss panels with Kagome cores. International Journal of Solids and Structures 2003;40: 6981–6988.

[7]. J. Xiong, B. Wang, L. Ma, J. Papadopoulos, A. Vaziri and L. Wu, Three-dimensional composite lattice structures fabricated by electrical discharge machining: Experimental mechanics 2013;54:405–412.

[8]. S. Yin, L. Wu and S. R. Nutt, Compressive efficiency of stretch-stretch-hybrid hierarchical composite lattice cores. Materials and Design 2014; 56:731–739.

[9]. M.Y.M, Zuhri, Z. Guan and W.J. Cantwell, The mechanical properties of natural fibre based honeycomb core structures. Composites Part B: Engineering 2014; 58:1-9.

[10]. F. Côté, V. S. Deshpande, N. A. Fleck and A. G. Evans, The compressive and shear responses of corrugated and diamond lattice materials. International Journal of Solids and Structures 2006; 6220-6242.

[11]. I. Dayyani, H.H. Khodaparast, B.K.S. Woods and M.I. Friswell, The design of a coated composite corrugated skin for the camber morphing airfoil. Journal of Intelligent Material Systems and Structures 2015; 26:1592-1608.

[12]. I. Dayyani, A.D. Shaw, E.L.S. Flores and M.I. Friswell, The mechanics of composite corrugated structures: A review with applications in morphing aircraft. Composite Structures 2015;133:358-380.

[13]. A.J. Malcom, M.T. Aronson, V.S. Deshpande and N.H.G. Wadley, Compressive response of glass fiber composite sandwich structures. Composites Part A – Applied Science and Manufacturing 2013;54:88-97.

[14]. S. Kazemahvazi, D. Tanner and D. Zenkert, Corrugated all-composite sandwich structures. Part 2: Failure mechanisms and experimental programme. Composites Science and Technology 2009;69:920-925.

[15]. M. R. M. Rejab and W. J. Cantwell, The mechanical behaviour of corrugated-core sandwich panels. Composites. Part B Engineering 2013;47:267–277.

[16]. F.N. Jin, H.L. Chen, L. Zhao, H.L. Fan, C.G. Cai and N. Kuang, Failure mechanisms of sandwich composites with orthotropic integrated woven corrugated cores: Experiments. Composite Structures 2013;98: 53-58.

[17]. C. Schneider, S. Kazemahvazi, D. Zenkert and V.S. Deshpande, Dynamic compression response of self-reinforced poly(ethylene terephthalate) composites and corrugated sandwich cores. Composites Part A: Applied Science and Manufacturing 2015:77:96-105.

[18]. Z. Hashin, Failure criteria for unidirectional fiber composites. Journal of Applied Mechanics 1980;47:329-334.

[19]. E. Sitnikova, Z.W. Guan, G.K. Schleyer, W.J.Cantwell, Modelling of perforation failure in fibre metal laminates subjected to high impulsive blast loading. International Journal of Solids and Structures 2014; 51: 3135-3146.

[20]. T. P. Vo, Z. W. Guan, W. J. Cantwell, G. K. Schleyer. Modelling of the low-impulse blast behaviour of fibre–metal laminates based on different aluminium alloys. Composites: Part B 2013;44: 141–151.

[21]. J. Zhou, Z. W. Guan and W. J. Cantwell, Modeling of the compression behavior of foam cores reinforced with composite rods, Polymer Composites 2015; DOI:10.1002/pc.23812.

[22]. J. X. Zhang, Q. H. Qin and T. J. Wang, Compressive strengths and dynamic response of corrugated metal sandwich plates with unfilled and foam-filled sinusoidal plate cores. Acta Mechanica 2013;224:759–775.

Table 1. Details of the glass fibre and carbon fibre reinforced epoxy composites

Prepreg	GFRP	CFRP
Fibre type	E-Glass	3k HTA
Weave style	Satin	Plain
Resin content (% wt)	40 ± 3	53 ± 3
Curing temperature (^{o}C)	125	125
Dwell time (minutes)	90	90
Laminate density (kg/m^{3})	1980	1780
Nominal thickness of ply (mm)	0.125	0.25

Table 2. Summary of material properties of two composites used in this study.

Properties	Symbol	(GFRP)	(CFRP)
Young's modulus in longitudinal direction	E_{11}	23 GPa	48 GPa
Young's modulus in transverse direction	E_{22}	23 GPa	48 GPa
Young's modulus in thickness	E_{33}	5 GPa	1 GPa
In-plane shear modulus	G_{12}	5 GPa	9 GPa
Through-thickness shear modulus	G_{13}, G_{23}	5 GPa	9 GPa
In-plane Poisson's ratio	v_{12}	0.15	0.1
Through-thickness Poisson's ratio	v_{13}, v_{23}	0.15	0.1
Longitudinal tensile strength	T_L	320 MPa	550 MPa
Longitudinal compressive strength	C_L	260 MPa	150 MPa
Transverse tensile strength	T_T	320 MPa	550 MPa
Transverse compressive strength	C_T	260 MPa	150 MPa
Transverse shear strength	S_T	100 MPa	120 MPa
Longitudinal shear strength	S_L	100 MPa	120 MPa

Table 3. Summary of the dimensions of the sandwich structures investigated in this study.

Specimen ID	No. of plies	Thickness 't' (mm)	Specimen Length (mm)	Specimen Width (mm)	Specimen Thickness (mm)	Core density (kg/m^3)
Test group 1: Varying corrugation thickness, t.						
GF1	2	0.25	80	20	20.75	38.7
GF2	4	0.5	80	20	21.5	77.7
GF3	6	0.75	80	20	22.25	116.6
GF4	8	1	80	20	23	155.4
GF5	10	1.25	80	20	23.75	194.3
CF1	1	0.25	80	20	20.75	34.9
CF2	2	0.5	80	20	21.5	69.9
CF3	3	0.75	80	20	22.25	104.8
CF4	4	1	80	20	23	139.7
CF5	5	1.25	80	20	23.75	174.7
Test group 2: Scaling effects for n = ¼, ½, ¾ and 1.						
GF6 (n=1/4)	2	0.25	40	10	10.75	77.7
GF7 (n=1/2)	4	0.5	80	20	21.5	77.7
GF8 (n=3/4)	6	0.75	120	30	32.25	77.7
GF9 (n=1)	8	1	160	40	43	77.7
CF6 (n=1/4)	1	0.25	40	10	10.75	69.9
CF7 (n=1/2)	2	0.5	80	20	21.5	69.9
CF8 (n=3/4)	3	0.75	120	30	32.25	69.9
CF9 (n=1)	4	1	160	40	43	69.9

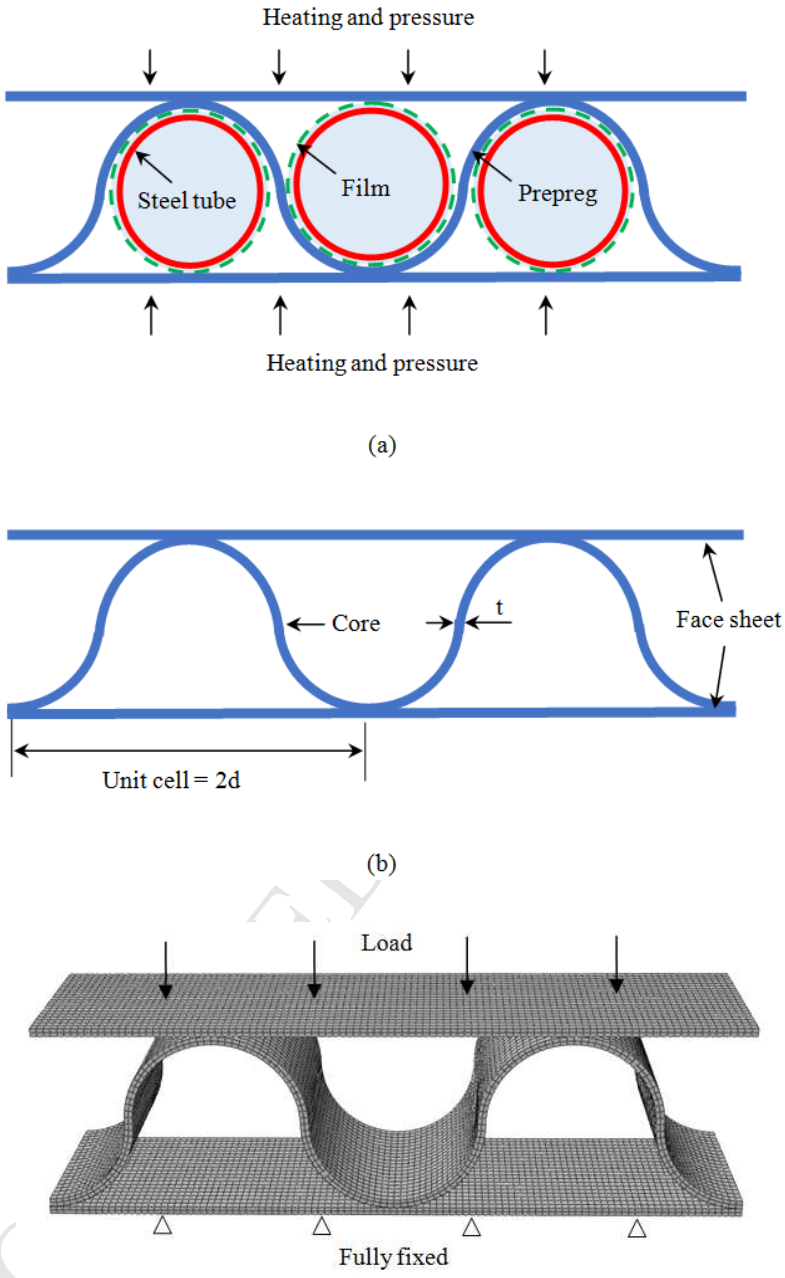

Figure 1. Schematic of the corrugated core sandwich structure. (a) showing the positioning of the steel cylinders and the Teflon film (dotted line) (b) the final structure following removal of the tubes and (c) finite element mesh of specimen CF2.

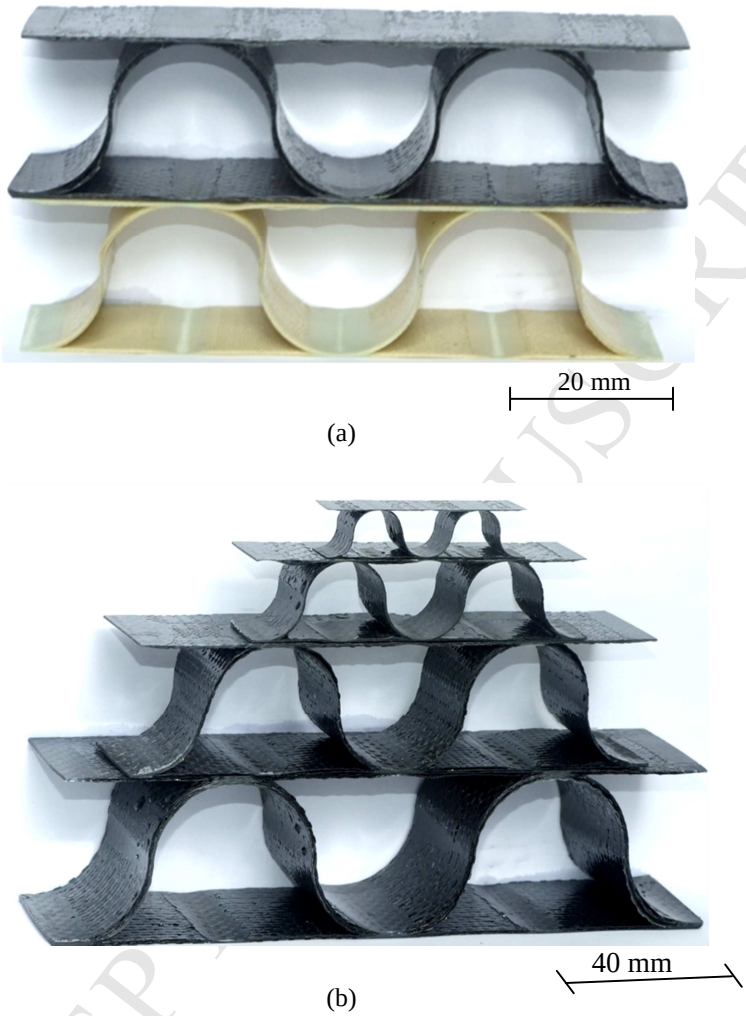

Figure 2. Photographs of the as-manufactured test specimens (a) the 20 mm CFRP sample CF3 (top) and the 20 mm GFRP sample GF3 (bottom) test samples and (b) the four scaled sizes of CFRP core (n=1/4, n=1/2, n=3/4 and n=1).

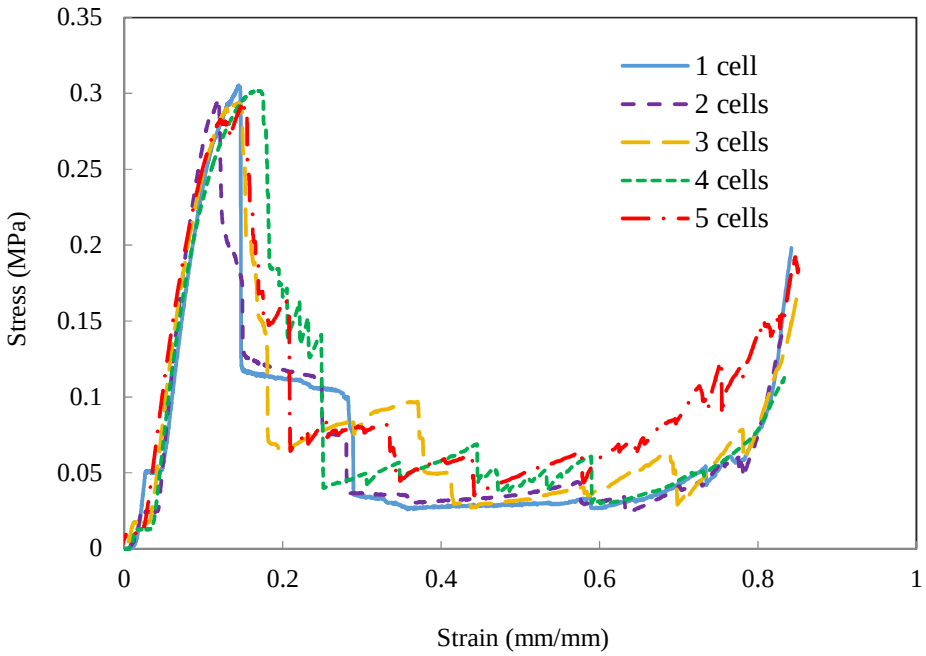

Figure 3. Comparison of the stress-strain traces for the corrugated GFRP samples ('d'=20 mm, 't' =0.5 mm) based on an increasing number of unit cells.

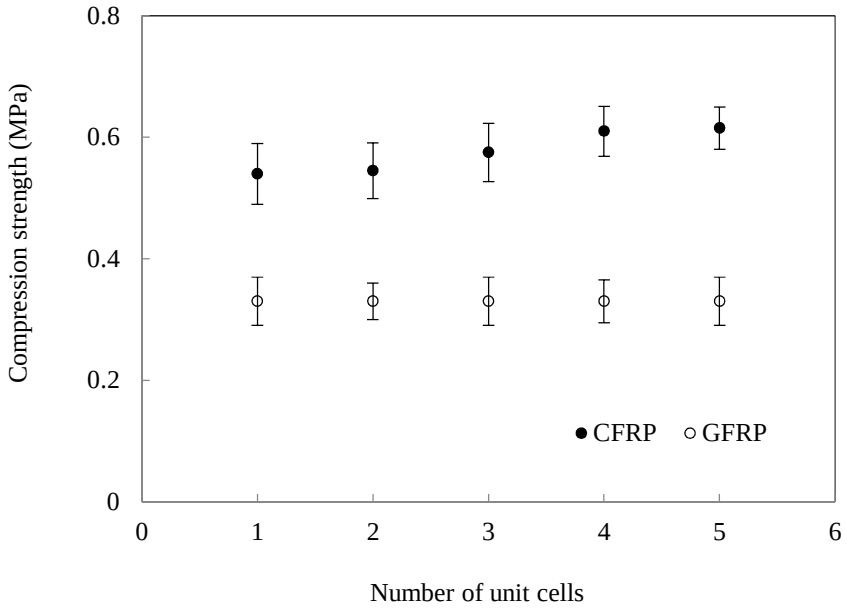

Figure 4. The influence of the number of unit cells on the compression properties of corrugated samples.

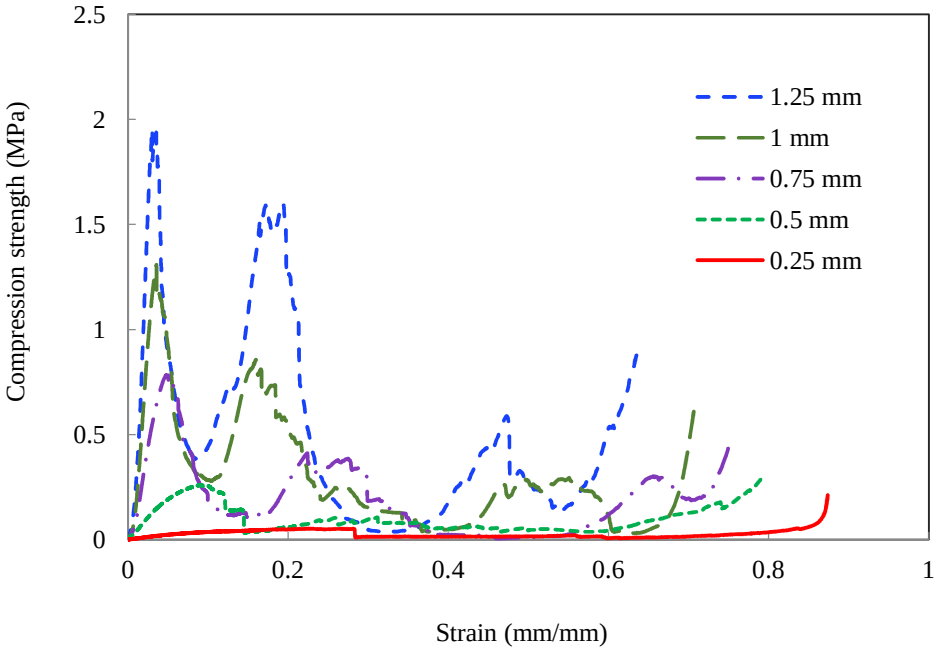

(a) GFRP

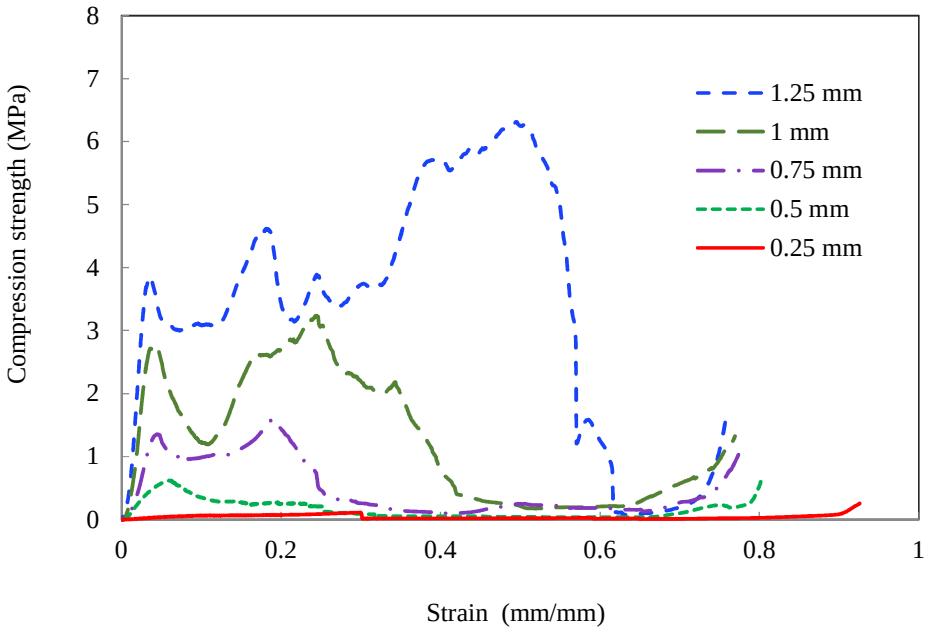

(b) CFRP

Figure 5. Compression stress-strain traces for GFRP (GF1 to GF5) and CFRP (CF1 to CF5) samples based on various corrugation thicknesses.

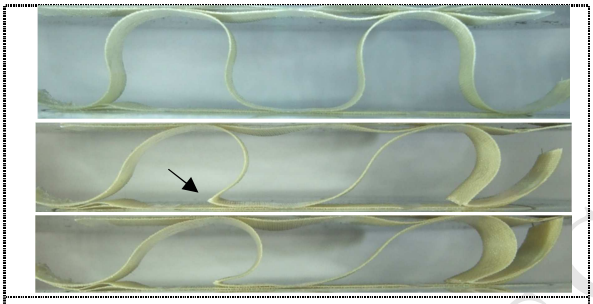

(a) Corrugation thickness = 0.25 mm (GF1).

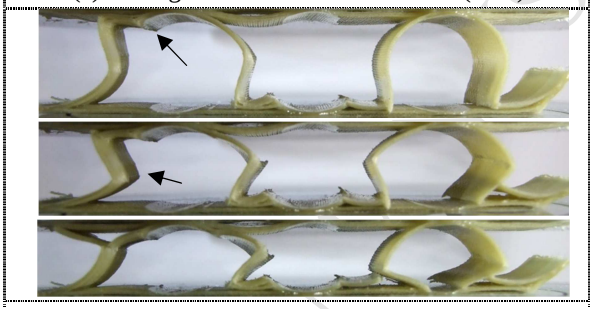

(b) Corrugation thickness = 0.75 mm (GF3).

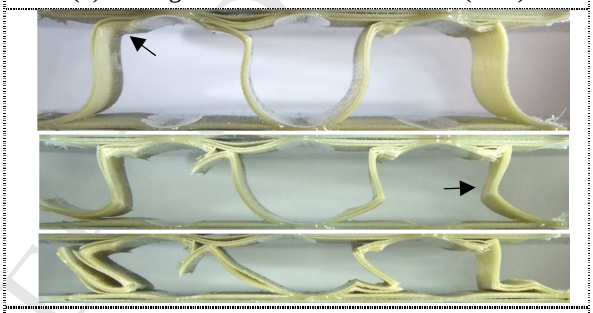

(c) Corrugation thickness = 1 mm (GF4).

Figure 6. Photographs showing the failure mechanisms in 20 mm thick GFRP cores. The arrows highlight examples of paths along which the composite failed.

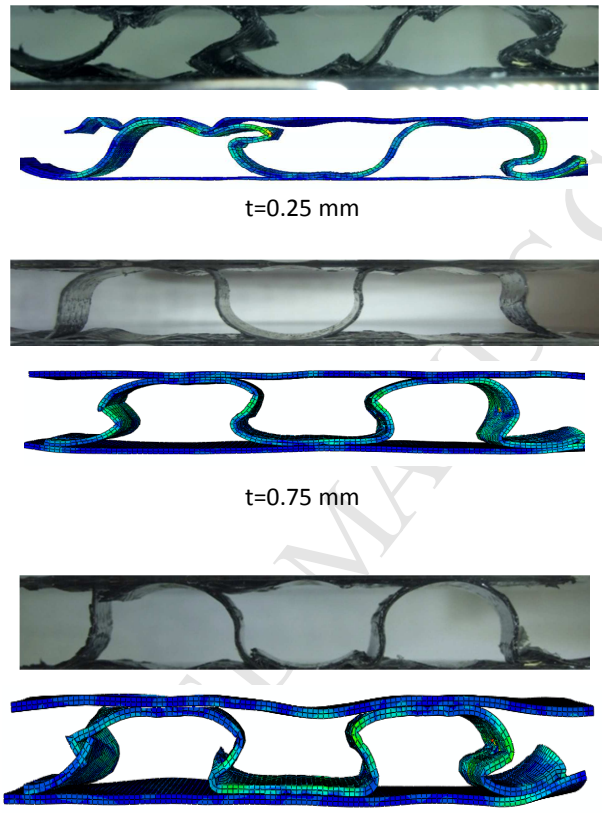

Figure 7. Comparison failure of CFRP samples based on an increasing wall thickness between FE and test.

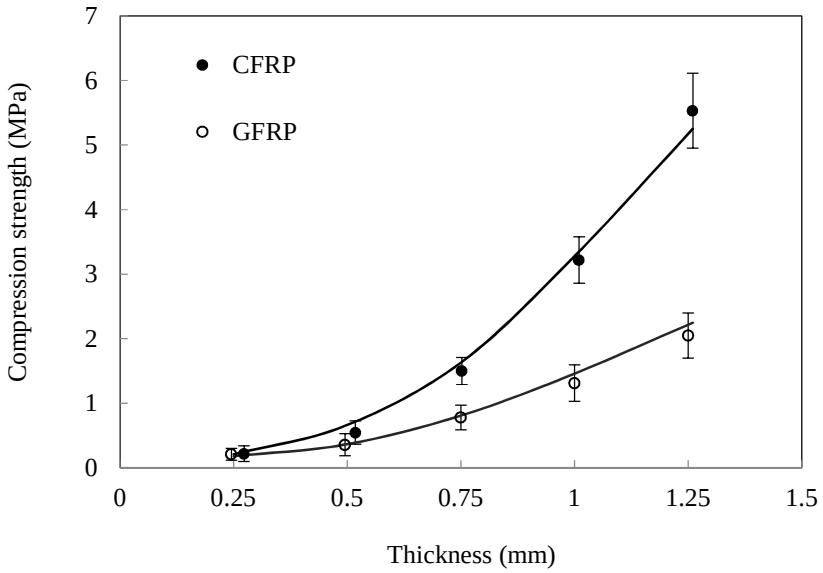

Figure 8. Compression strength versus corrugation thickness of the corrugation for GFRP and CFRP samples based on 20 mm diameter. The solid lines correspond to the FE predictions.

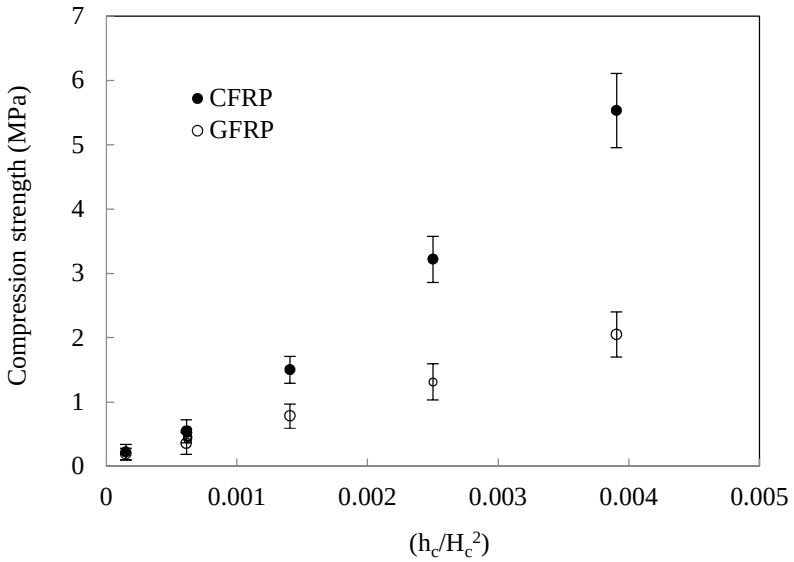

Figure 9. The variation of compression strength of the corrugated cores with $(h_c/H_c)^2$.

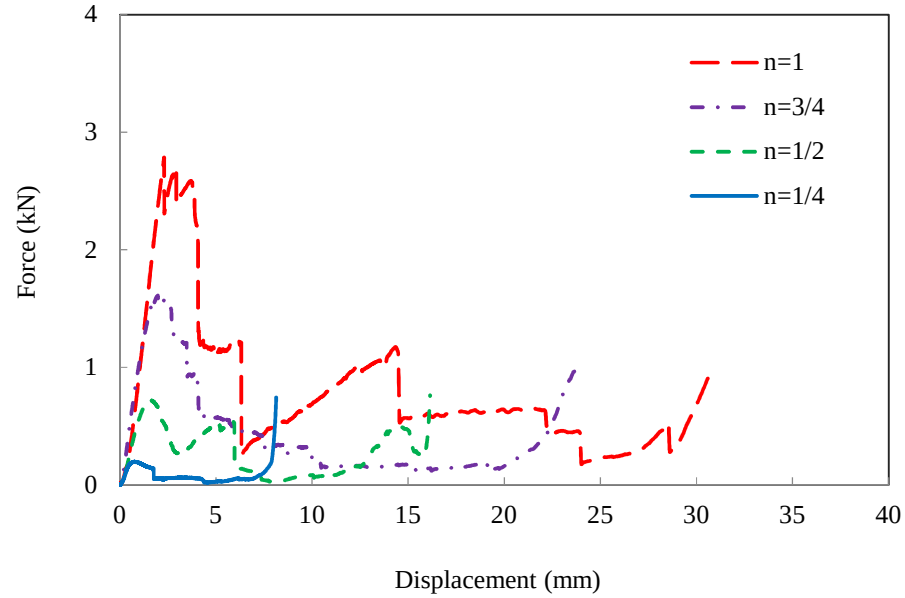

(a)

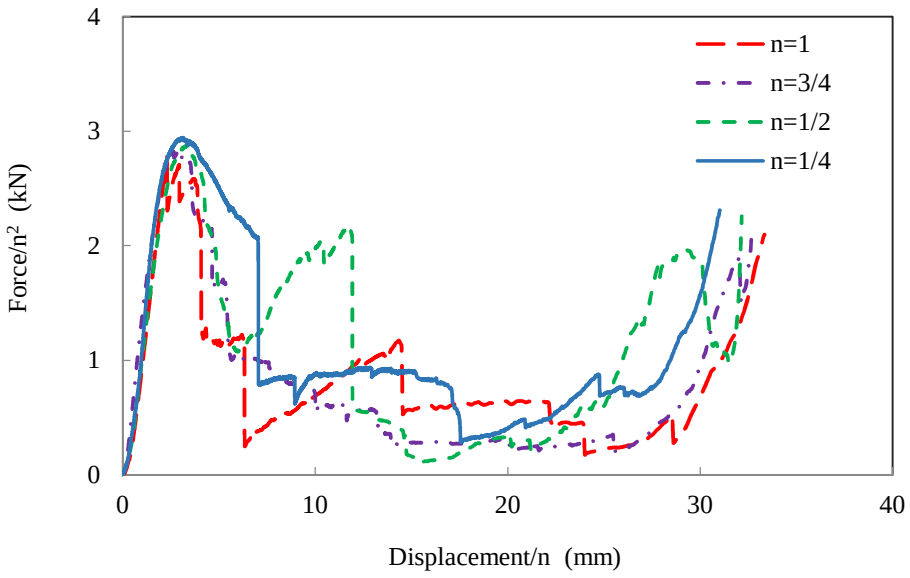

(b)

Figure 10. Compression tests on the GFRP samples (a) original force-displacement traces (b) scaled force-displacement traces. (Specimens GF6 to GF9).

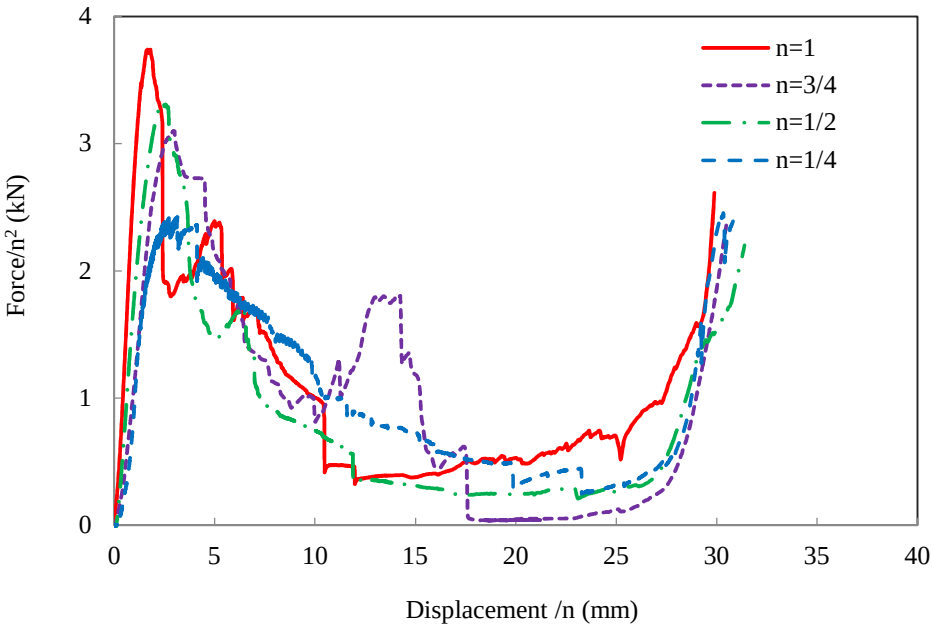

Figure 11. Compression tests on the CFRP samples, scaled force-displacement traces. (Specimens CF6 to CF9).

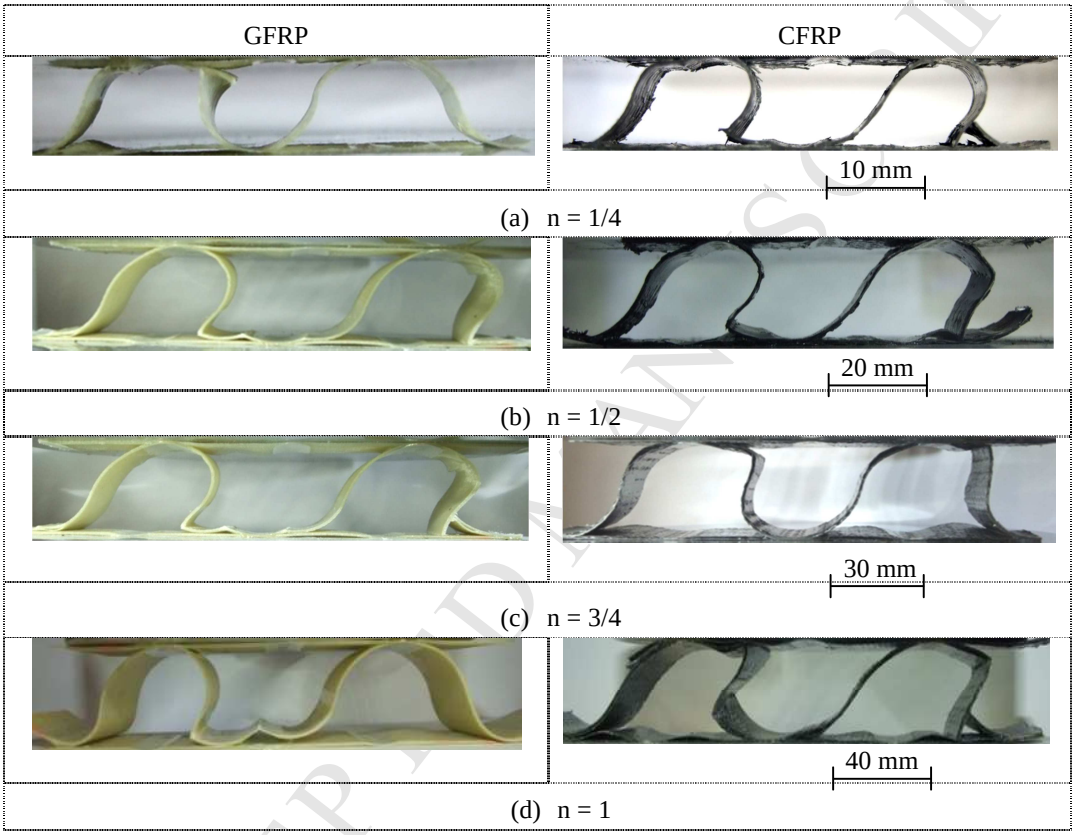

Figure 12. Photographs showing the failure mechanisms in the four scaled sizes of sample.

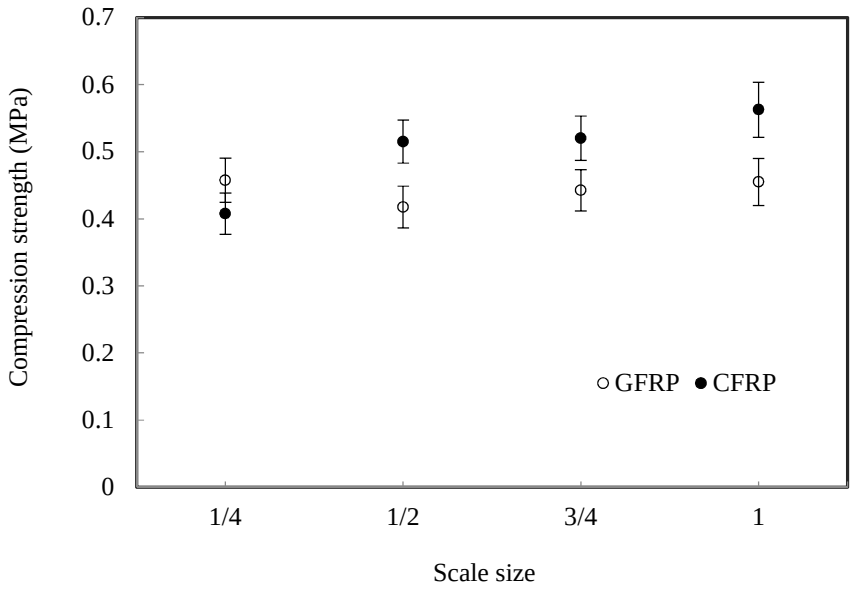

Figure 13. Compression strength versus scale size for scaled GFRP and CFRP samples following testing at a crosshead displacement rate of 4n mm/minute. The lines correspond to the FE predictions.